Interstudy reproducibility of dark blood high-resolution MRI in evaluating basilar atherosclerotic plaque at 3 Tesla

Luguang Chen ⓘ
Qi Liu ⓘ
Zhang Shi ⓘ
Xia Tian ⓘ
Wenjia Peng ⓘ
Jianping Lu ⓘ

PURPOSE
We aimed to evaluate the interscan, intraobserver, and interobserver reproducibility of basilar atherosclerotic plaque employing dark blood high-resolution magnetic resonance imaging (HR-MRI) at 3 Tesla.

METHODS
Sixteen patients (14 males and 2 females) with >30% basilar stenosis as identified by conventional magnetic resonance angiography were prospectively recruited for scan and rescan examinations on a 3 Tesla MRI system using T2-weighted turbo spin-echo protocol. Two observers independently measured the areas of vessels and lumens. Wall area was derived by subtracting the lumen area from the vessel area. Areas of vessels, lumens and walls were compared for the evaluation of interscan variability of basilar plaque. To assess the intraobserver variability, one observer reevaluated all the images of the first scan after a 4-week interval.

RESULTS
Fourteen patients were included in the final analysis. No clinically significant difference was observed for interscan, intraobserver, and interobserver measurements. The intraclass correlations for vessel, lumen, and wall areas were excellent and ranged from 0.973 to 0.981 for the interscan measurements, 0.997 to 0.998 for the intraobserver measurements and 0.979 to 0.985 for the interobserver measurements. The coefficients of variation for quantitative basilar morphology measurements were 4.31%–10.35% for the interscan measurements, 1.41%–4.62% for the intraobserver measurements and 3.79%–8.46% for the interobserver measurements. Compared with the interscan and interobserver measurements, narrow intervals of the scatterplots were observed for the intraobserver measurements by Bland-Altman plots.

CONCLUSION
Basilar atherosclerotic plaque imaging demonstrates excellent reproducibility at 3 Tesla. The study proves that dark blood HR-MRI may serve as a reliable tool for clinical studies focused on the progression and treatment response of basilar atherosclerosis.

I ntracranial atherosclerotic disease is a major cause of ischemic stroke all over the world, especially among patients of Asian and Hispanic ethnics (1, 2). A previous study reported that the incidence of intracranial atherosclerotic stenosis takes up 33% to 50% of stroke and transient ischemic attack (TIA) patients in China (3). Basilar atherosclerotic plaque usually occurs in patients with ischemic stroke and TIA of the posterior cerebral circulation (4). The atherosclerotic plaque component and remodeling of basilar artery, which are similar with coronary plaque (5), and the distribution of the plaque play a vital role in patients' treatment decision-making (6). The detailed assessment of plaque component is more significant to evaluate lumen stenosis exclusively, since atherosclerotic plaque formation and disruption may cause some hemodynamic changes on the vessel wall prior to the acute ischemic events (7).

Several luminal angiography techniques, such as digital subtraction angiography, computed tomography angiography and magnetic resonance angiography, have been employed to evaluate intracranial atherosclerotic stenosis, but these methods fail to delineate the vessel wall morphology properties and plaque components (4). Advanced magnetic

resonance imaging technology, especially at 3 Tesla (T) field strength, provides better signal-to-noise ratio (SNR), contrast-to-noise ratio (CNR) and image quality than those at 1.5 T (8, 9). Dark blood high-resolution magnetic resonance imaging (HR-MRI) has emerged in the last few years as a powerful technique for assessing plaque in the intracranial arteries (10–13). The following techniques have been used to enhance the dark blood effect and to have a better visualization of lumen and vessel wall of the arteries: saturation band (14), double inversion recovery (DIR) (15), quadruple inversion recovery (QIR) (16), motion-sensitized driven-equilibrium (MSDE) (17), and delay alternating with nutation for tailored excitation (DANTE) (18), each method with its merits and shortcomings. Compared with conventional angiography, HR-MRI has some merits in delineating the vessel wall characterization because of its noninvasive and radiation-free properties (4) and is more accurate in delineating basilar artery stenosis and detecting plaque (19). HR-MRI can be employed to discriminate between dissection and vasculitis (20), predict the progressive motor deficits after pontine infarction (21), investigate plaque enhancement (5, 22), and access the plaque distribution features and growth patterns of basilar artery (4, 6, 23–27). In addition, it has been used as an underlying guide for interventional treatment of intracranial atherosclerotic disease (28). Moreover, HR-MRI has been used for evaluating intraobserver and interobserver variability of intracranial arterial atherosclerotic plaques, such as carotid artery, middle cerebral artery and basilar artery (29–32). But above all, for the longitudinal study of atherosclerosis, the repeated HR-MRI scans can be used to monitor variations in vessel wall and may reflect the treatment response (9, 32, 33). We hypothesized that the interscan reproducibility of basilar artery plaque imaging was excellent using HR-MRI at 3 T. However,

to the best of our knowledge, little has been reported on the scan and rescan reproducibility of quantitative *in vivo* measurements of basilar artery plaque using two-dimensional (2D) T2-weighted protocol.

Therefore, the purpose of the current study was to evaluate the interscan, intraobserver and interobserver reproducibility of basilar artery plaque employing dark blood HR-MRI at 3 T.

Methods

Subjects

Sixteen consecutive patients (14 males and 2 females; age, 54–67 years; mean age, 61.9±3.9 years) with basilar artery atherosclerosis were prospectively recruited from February 2014 to July 2014. Both symptomatic and asymptomatic subjects with >30% stenosis of basilar artery as identified by conventional contrast-enhanced magnetic resonance angiography were included in the current study, the degree of stenosis was assessed using Warfarin-Aspirin Symptomatic Intracranial Disease (WASID) method by a radiologist who has an experience of >20 years in the diagnostic neuroradiology (34). Patients were deemed to be symptomatic if they had ischemic stroke or TIA in the basilar artery territory during the last 4 weeks; however, if they did not have a history of cerebrovascular events or if an ischemic event occurred in a vascular distribution beyond the stenotic basilar artery, they were regarded as asymptomatic patients (31). Ten patients were symptomatic, and the others were asymptomatic. The following criteria were used to exclude patients: 1) normal or <30% stenotic arteries at the site of the basilar artery; 2) nonatherosclerotic vasculopathy; 3) arteritis; 4) claustrophobia; and 5) poor image quality for interpretation. Two patients were excluded from the final inclusion because of poor image quality (scores, ≤2) and uncooperative examination. Therefore, fourteen patients were included in the final analysis. The study was approved by our local institutional review board, and each patient gave written informed consent.

Magnetic resonance imaging

All imaging was performed using a 3 T whole-body MRI system (Skyra, Siemens medical solution, Germany), with a peak gradient strength of 45 mT/m and a slew rate of 200 mTm^{-1}ms^{-1}. The integrated body coil was employed for radiofrequency transmission, and a standard 20-channel head/

neck coil was used for magnetic resonance signal reception. All patients were examined in the supine position with eyes positioned at the center of the magnet. In addition, two soft cushions were inserted between the head and coil to help the subject's head immobile. Two protocols were used: three-dimensional (3D) time-of-flight images were obtained using repetition time/echo time (TR/TE) 21/3.4 ms, field of view (FOV) 180×200 mm^2, matrix 330×384, thickness 0.7 mm, and average 1; 2D T2-weighted turbo spin-echo (TSE) images were obtained using TR/TE 2890/46 ms, FOV 100×100 mm^2, matrix 256×320, thickness 2 mm, Gap 0.5 mm, Slices 12, turbo factor 20, and averages 2. Fat saturation was applied to suppress signal from adjacent fatty tissues and improve identification of vessel wall boundaries. The dark blood technique with a regional saturation pulse of 60 mm thickness was used to saturate the inflow arterial signal. All patients underwent two repeated scans of the basilar artery vessel wall during two different scan sessions. After the first scan (Scan 1), the coil was removed, the patient was allowed to have a short rest outside the scanner, following which he/she was repositioned for the second scan (Scan 2). The total time of two scan sessions and scan interval was approximately 30 minutes.

Image analysis

Cross-sectional images were used to perform image analysis and quantitative analysis, with a total of 58 data points from 14 patients. The images of all subjects were transferred to an advanced workstation for analysis. The vessel wall images of basilar artery acquired using T2-weighted TSE protocol at the two different scan sessions were evaluated and scored for image quality by an observer with 4 years of experience in neuroradiology, who was blinded to the subject identity and scan session of each patient. The grade of image quality was based on the following four criteria: overall image quality, vessel wall delineation, flow suppression, and artifacts (35), each scored on a 5-point scale (1= poor; 5= excellent). If all scores were ≥3, the image qualified for further evaluation.

Quantitative analysis

Area measurements were performed by two independent observers on the cross-sectional T2-weighted images of both scan series. Images of repeated scans of each patient were analyzed in a random-
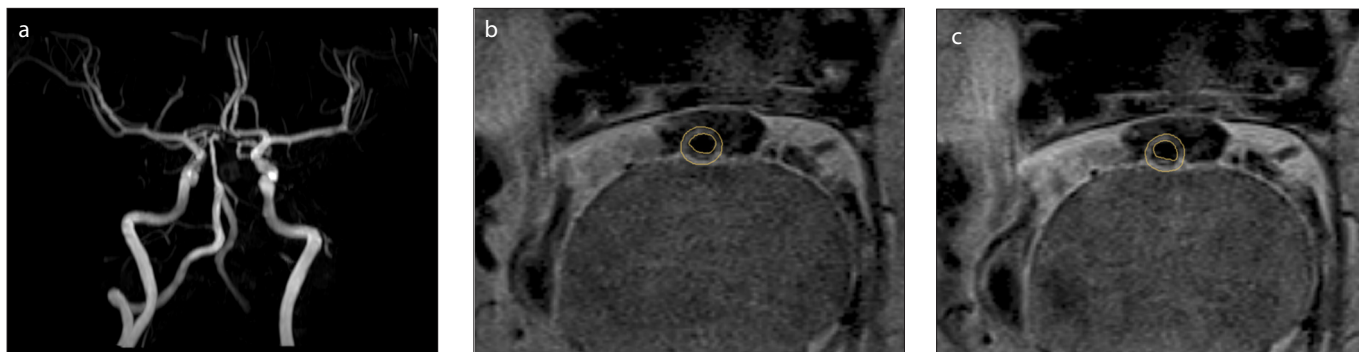
Figure 1. a–c. Example of interscan analysis of vessel wall and lumen boundaries for basilar artery: Panel **(a)** shows 3D time-of-flight magnetic resonance angiography (Scan 1); panel **(b)** shows 2D T2-weighted TSE (Scan 1) **(b)**; panel **(c)** shows 2D T2-weighted TSE (Scan 2).

Table 1. Interscan reproducibility for basilar artery

	Scan 1 (mean±SD)	Scan 2 (mean±SD)	ICC (95% CI)	CV (%)
Vessel area (mm^2)	27.37±7.24	27.51±7.14	0.973 (0.954–0.984)	4.31
Lumen area (mm^2)	4.54±3.25	4.39±3.04	0.979 (0.965–0.988)	10.35
Wall area (mm^2)	22.82±8.62	23.12±8.65	0.981 (0.968–0.989)	5.26

SD, standard deviation of mean; ICC, intraclass correlation coefficient; CI, confidence interval; CV, coefficient of variation.

Table 2. Intraobserver reproducibility for basilar artery

	Measurement 1 (mean±SD)	Measurement 2 (mean±SD)	ICC (95% CI)	CV (%)
Vessel area (mm^2)	27.37±7.24	27.27±7.18	0.997 (0.995–0.998)	1.41
Lumen area (mm^2)	4.54±3.25	4.49±3.20	0.996 (0.993–0.998)	4.62
Wall area (mm^2)	22.82±8.62	22.78±8.60	0.997 (0.995–0.998)	1.95

SD, standard deviation of mean; CI, confidence interval; ICC, intraclass correlation coefficient; CV, coefficient of variation.

ized order to avoid any potential bias. The vessel and lumen boundaries were manually outlined for each image and area measurements were performed employing a dedicated display software (CMRTools, Cardiovascular Imaging Solutions; Fig. 1). Wall area was determined by subtracting the lumen area from the vessel area. To assess intraobserver variability, the first observer reevaluated the cross-sectional T2-weighted images of the first scan. Area measurements were performed twice during the two sessions which were separated by a 4-week interval and presented in a different order to avoid any recall bias.

Statistical analysis

All analyses were performed using the SPSS software for windows (version 16.0, SPSS Inc.). Quantitative data were described as means ± standard deviation. The coefficient of variation (CV) was de- termined by the standard deviation (SD) of the two matched measurements of T2-weighted images divided the mean of those measurements (CV = SD/mean × 100%). Intraclass correlation coefficient (ICC) was calculated using two-way mixed model and single consistency type to assess the agreement between repeated measurements, and values were graded according to the method proposed by Shout and Fleiss (36): <0.4, poor agreement; 0.4–0.75, good agreement; >0.75, excellent agreement. In addition, Bland-Altman plots (37) were also used to determine the interscan, intraobserver and interobserver agreement of area measurements, which illustrated the level of agreement by plotting the differences between the two area measurements against the mean of the two area measurements. A type-I error level of 5% was used for making statistical inferences.

Results

The results for scan and rescan reproducibility are presented in Table 1. The areas for the two examinations were 27.37±7.24 mm^2 and 27.51±7.14 mm^2 for vessel measurements, 4.54±3.25 mm^2 and 4.39±3.04 mm^2 for lumen measurements, as well as 22.82±8.62 mm^2 and 23.12±8.65 mm^2 for wall measurements, respectively, which showed no clinically significant difference between these measurements. The interscan reproducibility was excellent and the ICCs and CVs for vessel, lumen, and wall area measurements were 0.973 and 4.31%, 0.979 and 10.35%, and 0.981 and 5.26%, respectively. Excellent agreement was also observed for scan and rescan reproducibility employing Bland-Altman plots (Fig. 2).

The statistical results for the intraobserver reproducibility are presented in Table 2. The areas for the intraobserver measurement were 27.37±7.24 mm^2 and 27.27±7.18 mm^2 for vessels, 4.54±3.25 mm^2 and 4.49±3.20 mm^2 for lumens, as well as 22.82±8.62 mm^2 and 22.78±8.60 mm^2 for walls, respectively, which showed no clinically significant difference between these measurements. The intraobserver reproducibility was excellent and the ICCs and CVs for vessel, lumen and wall area measurements were 0.997 and 1.41%, 0.996 and 4.62%, and 0.997 and 1.95%, respectively. Excellent agreement was also observed for intraobserver reproducibility employing Bland-Altman plots (Fig. 3).

The statistical results for the interobserver reproducibility are presented in Table 3. The areas for the interobserver measurement were 27.37±7.24 mm^2 and 27.48±7.21 mm^2 for vessels, 4.54±3.25 mm^2 and 4.63±3.10 mm^2 for lumens, as well as 22.82±8.62 mm^2 and 22.85±8.69 mm^2 for walls, respectively, with no clinically significant difference between these measurements. The interobserver repro-
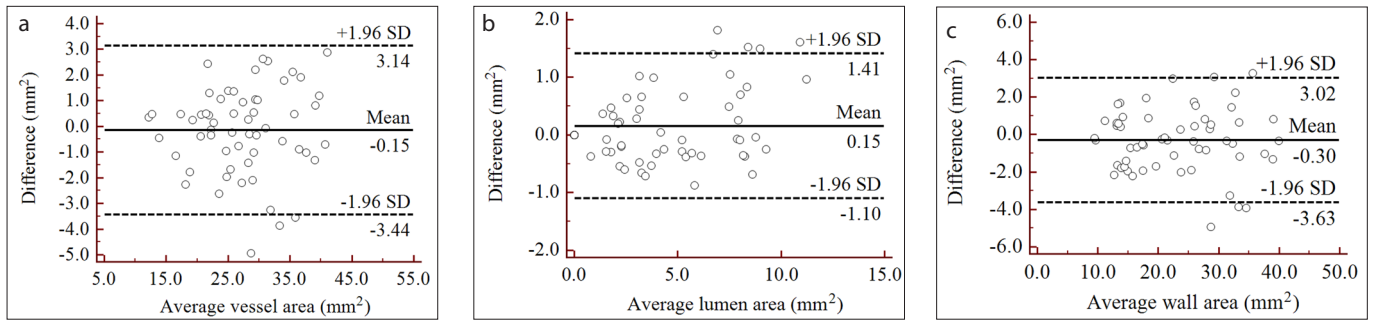
Figure 2. a–c. Bland-Altman plots of interscan reproducibility for vessel area (**a**), lumen area (**b**), and wall area (**c**) measurements of basilar artery plaque, respectively. Dashed lines represent the limits of agreement.
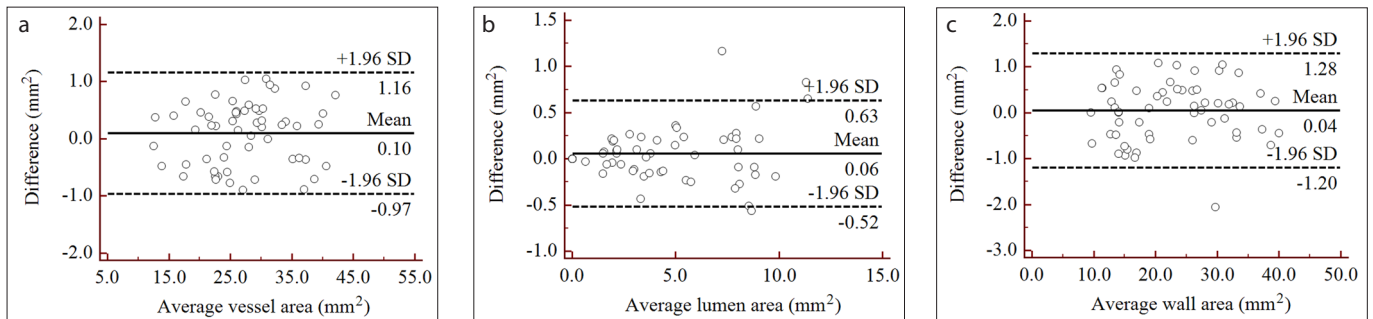
Figure 3. a–c. Bland-Altman plots of intraobserver reproducibility for vessel area (**a**), lumen area (**b**), and wall area (**c**) measurements of basilar artery plaque, respectively. Dashed lines represent the limits of agreement.
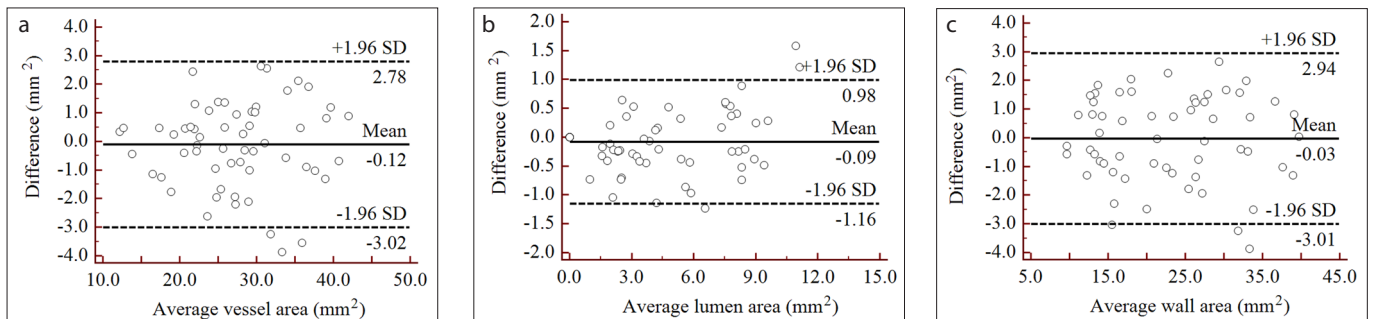
Figure 4. a–c. Bland-Altman plots of interobserver reproducibility for vessel area (**a**), lumen area (**b**), and wall area (**c**) measurements of basilar artery plaque, respectively. Dashed lines represent the limits of agreement.

Table 3. Interobserver reproducibility for basilar artery

	Observer 1 (mean±SD)	Observer 2 (mean±SD)	ICC (95% CI)	CV (%)
Vessel area (mm^2)	27.37±7.24	27.48±7.21	0.979 (0.965–0.988)	3.79
Lumen area (mm^2)	4.54±3.25	4.63±3.10	0.985 (0.975–0.991)	8.46
Wall area (mm^2)	22.82±8.62	22.85±8.69	0.985 (0.974–0.991)	4.66

SD, standard deviation of the mean; ICC, intraclass correlation coefficient; CI, confidence interval; CV, coefficient of variation.

ducibility was excellent and the ICCs and CVs for vessel, lumen, and wall area measurements were 0.979 and 3.79%, 0.985 and 8.46%, and 0.985 and 4.66%, respectively. Excellent agreement was also observed for interobserver reproducibility employing Bland-Altman plots (Fig. 4).

Discussion

Our study shows that vessel, lumen and wall area measurements of basilar artery plaques using dark blood HR-MRI had excellent reproducibility for interscan, interobserver, and intraobserver measurements, respectively (32).

The present study showed that the ICCs of interscan and interobserver variability were excellent for vessel, lumen, and wall area measurements (ICC range: 0.973–0.981, 0.979–0.985, respectively). Moreover, the CVs of these measurements ranged from 4.31% to 10.35% and 3.79% to 8.46% for interscan and interobserver variability, respectively. Yet the lumen measurements had the largest CV in evaluating interscan variability. As expected, intraobserver reproducibility was superior to interscan and interobserver reproducibility. Compared with the interscan and interobserver variability, intraobserver measurements had larger ICCs (range, 0.996–0.997) for assessing vessel, lumen and wall areas, and all CVs were <5.00%. Ma et al. (29) reported the in-

terobserver and intraobserver reproducibility of basilar atherosclerotic plaque at the level of the trigeminal ganglion; their images were acquired at one scan session and they only assessed wall area measurement. They found intraobserver reproducibility was excellent for wall measurement with an ICC of 0.973, which is consistent with our result. To the best of our knowledge, no study had evaluated the interscan reproducibility of basilar plaque before. Li et al. (38) found that there was high reliability for carotid morphology measurements using HR-MRI in a scan and rescan study. In another study, Zhang et al. (33) reported scan-rescan reproducibility for middle cerebral artery plaque morphology measurements using HR-MRI at 3 T. They found excellent reproducibility for area measurements with CV ranging from 6.1% to 11.8%; in addition, their results showed a larger CV for lumen area measurements than other morphologic parameters, which is similar to our results. We speculated three possible reasons: First, it was very hard for the technologist to keep the same slice positioning for each patient during the two scan sessions, and quantitative measurement of lumen area was more sensitive to positioning error than that of wall and vessel areas. Second, due to the different diameters of lumens and vessels, the relative error of lumen area measurement was larger than that of vessel area when performing multiple measurements. Third, the spatial resolution may also play an important role in quantifying area measurements. In our study, we used a highly nonisotropic spatial resolution of 0.31 mm × 0.39 mm × 2.00 mm for imaging basilar atherosclerotic plaque, and the slice thickness was much larger than the in-plane resolution, which was likely to result in image misregistration (38). In addition, Bland-Altman plots showed an excellent agreement for interscan, intraobserver, and interobserver measurements; however, compared with the interscan and interobserver measurements, narrow intervals of the scatterplots were observed for the intraobserver measurements (Figs. 2 and 3).

A previous study of carotid atherosclerosis reported that the SNR and CNR of the images acquired at 3 T were significantly better in comparison with the images acquired at 1.5 T in terms of interscan reproducibility (9). Their conclusion was in agreement with another study by Yarnykh et al. (8), where 3 T MRI was shown to have a number of benefits for carotid plaque imaging including increased SNR, higher spatial resolution, and a reduction of examination time (8). Therefore, in the present study we employed 3 T HR-MRI for assessing morphology measurement of basilar atherosclerotic plaque. Zhu et al. (39) found that high-resolution intracranial vessel wall imaging at 7 T is superior to 3 T in terms of improved image quality and diagnostic performance using 3D T1-weighted fast spin-echo (39). However, 7 T MRI system has not been widely approved to use in clinical settings, and 3 T MRI is commonly used to explore *in vivo* atherosclerotic plaque (10, 12, 28). Several techniques have been used to improve dark blood effect, such as saturation band (14), DIR (15), QIR (16), MSDE (17), and DANTE (18). Due to the inherent flow void effect of turbo spin-echo, in the present study we used saturation band to saturate the inflow blood signal when imaging basilar plaque because of its simplicity and low specific absorption ratio properties.

Recently, several studies have evaluated the intracranial vessel wall using 3D HR-MRI which offers larger imaging coverage, higher spatial resolution and improved SNR. However, those studies focused mainly on T1-weighted or proton-density-weighted vessel wall imaging (26, 40, 41). In our study, dark blood high-resolution T2-weighted images were chosen for quantitative measurement, since contrast levels between the lumen and plaque, the vessel wall and cerebrospinal fluid were higher than those seen in other scanning protocols (31). Moreover, flow compensation in the slice direction was also used to decrease pulsation artifacts (31). To minimize errors caused by slice positioning during the repeated examinations, 3D scanning protocols with isotropic spatial resolution, high SNR and large coverage may be used; however, 3D technique needs long acquisition time and is vulnerable to motion artifacts. Therefore, fast imaging techniques are required to cut down the scan time. In the present study, excellent reproducibility was observed for repeated HR-MRI examinations of basilar artery plaque, which is vitally important for assessing the progression of basilar atherosclerosis and monitoring the treatment response on basilar atherosclerotic disease. In addition, reliable assessment of serial scans is paramount to identify the composition of basilar atherosclerotic plaque in clinical practice.

There are several limitations to the present study. First, the sample size is relatively small. Due to poor image quality in 3 patients, 14 patients were involved to the final analysis. A larger sample size is needed to validate the present findings in future studies. Second, we manually traced the vessel wall and lumen boundaries on the T2-weighted images to assess the variability of the repeated measurements. However, an automated vessel wall analysis tool is needed and may reduce errors between the interscan and intraobserver measurements. Finally, there was a short scan session interval between the repeated examinations, which took approximately 10 minutes.

In conclusion, basilar atherosclerotic plaque imaging demonstrates excellent reproducibility at 3 T. Our study suggests that dark blood HR-MRI may serve as a reliable tool for clinical studies focused on the progression and treatment response of basilar atherosclerosis.

Financial disclosure

Conflict of interest disclosure

The authors declared no conflicts of interest.

References

1. Gorelick PB, Wong KS, Bae HJ, Pandey DK. Large artery intracranial occlusive disease: a large worldwide burden but a relatively neglected frontier. Stroke 2008; 39:2396–2399. [CrossRef]
2. De Silva DA, Woon FP, Lee MP, Chen CP, Chang HM, Wong MC. South Asian patients with ischemic stroke: intracranial large arteries are the predominant site of disease. Stroke 2007; 38:2592–2594. [CrossRef]
3. Wong LK. Global burden of intracranial atherosclerosis. Int J Stroke 2006; 1:158–159. [CrossRef]
4. Huang B, Yang WQ, Liu XT, Liu HJ, Li PJ, Lu HK. Basilar artery atherosclerotic plaques distribution in symptomatic patients: a 3.0T high-resolution MRI study. Eur J Radiol 2013; 82:e199–203. [CrossRef]
5. Wang W, Yang Q, Li D, et al. Incremental value of plaque enhancement in patients with moderate or severe basilar artery stenosis: 3.0 T high-resolution magnetic resonance study. Biomed Res Int 2017; 2017:4281629.
6. Yu J, Li ML, Xu YY, et al. Plaque distribution of low-grade basilar artery atherosclerosis and its clinical relevance. BMC Neurol 2017; 17:8. [CrossRef]
7. Chen JW, Wasserman BA. Vulnerable plaque imaging. Neuroimaging Clin N Am 2005; 15:609–621, xi. [CrossRef]
8. Yarnykh VL, Terashima M, Hayes CE, et al. Multicontrast black-blood MRI of carotid arteries: comparison between 1.5 and 3 Tesla magnetic field strengths. J Magn Reson Imaging 2006; 23:691–698. [CrossRef]
9. Vidal A, Bureau Y, Wade T, et al. Scan-rescan and intra-observer variability of magnetic resonance imaging of carotid atherosclerosis at 1.5 T and 3.0 T. Phys Med Biol 2008; 53:6821–6835. [CrossRef]

10. Chung GH, Kwak HS, Hwang SB, Jin GY. High-resolution MR imaging in patients with symptomatic middle cerebral artery stenosis. Eur J Radiol 2012; 81:4069–4074. [CrossRef]

11. Li ML, Xu WH, Song L, et al. Atherosclerosis of middle cerebral artery: evaluation with high-resolution MR imaging at 3T. Atherosclerosis 2009; 204:447–452. [CrossRef]

12. Ryu CW, Kwak HS, Jahng GH, Lee HN. High-resolution MRI of intracranial atherosclerotic disease. Neurointervention 2014; 9:9–20. [CrossRef]

13. Lou X, Ma N, Shen H, Shi KN, Jiang WJ, Ma L. Noninvasive visualization of the basilar artery wall and branch ostia with high-resolution three-dimensional black-blood sequence at 3 Tesla. J Magn Res Imaging 2014; 39:911–916. [CrossRef]

14. Felmlee JP, Ehman RL. Spatial presaturation: a method for suppressing flow artifacts and improving depiction of vascular anatomy in MR imaging. Radiology 1987; 164:559–564. [CrossRef]

15. Yarnykh VL, Yuan C. Multislice double inversion-recovery black-blood imaging with simultaneous slice reinversion. J Magn Reson Imaging 2003; 17:478–483. [CrossRef]

16. Yarnykh VL, Yuan C. T1-insensitive flow suppression using quadruple inversion-recovery. Magn Reson Med 2002; 48:899–905. [CrossRef]

17. Wang J, Yarnykh VL, Hatsukami T, Chu B, Balu N, Yuan C. Improved suppression of plaque-mimicking artifacts in black-blood carotid atherosclerosis imaging using a multislice motion-sensitized driven-equilibrium (MSDE) turbo spin-echo (TSE) sequence. Magn Reson Med 2007; 58:973–981. [CrossRef]

18. Li L, Miller KL, Jezzard P. DANTE-prepared pulse trains: a novel approach to motion-sensitized and motion-suppressed quantitative magnetic resonance imaging. Magn Reson Med 2012; 68:1423–1438. [CrossRef]

19. Kim YS, Lim SH, Oh KW, et al. The advantage of high-resolution MRI in evaluating basilar plaques: a comparison study with MRA. Atherosclerosis 2012; 224:411–416. [CrossRef]

20. Swartz RH, Bhuta SS, Farb RI, et al. Intracranial arterial wall imaging using high-resolution 3-tesla contrast-enhanced MRI. Neurology 2009; 72:627–634. [CrossRef]

21. Lim SH, Choi H, Kim HT, et al. Basilar plaque on high-resolution MRI predicts progressive motor deficits after pontine infarction. Atherosclerosis 2015; 240:278–283. [CrossRef]

22. Qiao Y, Zeiler SR, Mirbagheri S, et al. Intracranial plaque enhancement in patients with cerebrovascular events on high-spatial-resolution MR images. Radiology 2014; 271:534–542. [CrossRef]

23. Ma N, Jiang WJ, Lou X, et al. Arterial remodeling of advanced basilar atherosclerosis: a 3-tesla MRI study. Neurology 2010; 75:253–258. [CrossRef]

24. Feng C, Hua T, Xu Y, Liu XY, Huang J. Arterial remodeling of basilar atherosclerosis in isolated pontine infarction. Neurol Sci 2015; 36:547–551. [CrossRef]

25. Xu WH, Li ML, Gao S, et al. Plaque distribution of stenotic middle cerebral artery and its clinical relevance. Stroke 2011; 42:2957–2959. [CrossRef]

26. Chen Z, Liu AF, Chen H, et al. Evaluation of basilar artery atherosclerotic plaque distribution by 3D MR vessel wall imaging. J Magn Reson Imaging 2016; 44:1592–1599. [CrossRef]

27. Zhu X, Liu L, He X, et al. Wall thickening pattern in atherosclerotic basilar artery stenosis. Neurol Sci 2016; 37:269–276. [CrossRef]

28. Jiang WJ, Yu W, Ma N, Du B, Lou X, Rasmussen PA. High resolution MRI guided endovascular intervention of basilar artery disease. J Neurointerv Surg 2011; 3:375–378. [CrossRef]

29. Ma N, Lou X, Zhao TQ, Wong EH, Jiang WJ. Intraobserver and interobserver variability for measuring the wall area of the basilar artery at the level of the trigeminal ganglion on high-resolution MR images. AJNR Am J Neuroradiol 2011; 32:E29–32. [CrossRef]

30. Touze E, Toussaint JF, Coste J, et al. Reproducibility of high-resolution MRI for the identification and the quantification of carotid atherosclerotic plaque components: consequences for prognosis studies and therapeutic trials. Stroke 2007; 38:1812–1819. [CrossRef]

31. Yang WQ, Huang B, Liu XT, Liu HJ, Li PJ, Zhu WZ. Reproducibility of high-resolution MRI for the middle cerebral artery plaque at 3T. Eur J Radiol 2014; 83:e49–55. [CrossRef]

32. Kroner ES, Westenberg JJ, van der Geest RJ, et al. High field carotid vessel wall imaging: a study on reproducibility. Eur J Radiol 2013; 82:680–685. [CrossRef]

33. Zhang X, Zhu C, Peng W, et al. Scan-rescan reproducibility of high resolution magnetic resonance imaging of atherosclerotic plaque in the middle cerebral artery. PLoS One 2015; 10:e0134913. [CrossRef]

34. Samuels OB, Joseph GJ, Lynn MJ, Smith HA, Chimowitz MI. A standardized method for measuring intracranial arterial stenosis. AJNR Am J Neuroradiol 2000; 21:643–646.

35. Hatsukami TS, Ross R, Polissar NL, Yuan C. Visualization of fibrous cap thickness and rupture in human atherosclerotic carotid plaque in vivo with high-resolution magnetic resonance imaging. Circulation 2000; 102:959–964. [CrossRef]

36. Shrout PE, Fleiss JL. Intraclass correlations: uses in assessing rater reliability. Psychol Bull 1979; 86:420–428. [CrossRef]

37. Bland JM, Altman DG. Statistical methods for assessing agreement between two methods of clinical measurement. Lancet 1986; 1:307–310. [CrossRef]

38. Li F, Yarnykh VL, Hatsukami TS, et al. Scan-rescan reproducibility of carotid atherosclerotic plaque morphology and tissue composition measurements using multicontrast MRI at 3T. J Magn Reson Imaging 2010; 31:168–176. [CrossRef]

39. Zhu C, Haraldsson H, Tian B, et al. High resolution imaging of the intracranial vessel wall at 3 and 7 T using 3D fast spin echo MRI. MAGMA 2016; 29:559–570. [CrossRef]

40. Li ML, Xu YY, Hou B, et al. High-resolution intracranial vessel wall imaging using 3D CUBE T1 weighted sequence. Eur J Radiol 2016; 85:803–807. [CrossRef]

41. Zhu XJ, Jiang WJ, Liu L, Hu LB, Wang W, Liu ZJ. Plaques of nonstenotic basilar arteries with isolated pontine infarction on three-dimensional high isotropic resolution magnetic resonance imaging. Chin Med J (Engl) 2015; 128:1433–1437. [CrossRef]